Comparison of pin-fin and finned shape heat sink for power electronics in future aircraft

Assel Sakanova*[1]

[1]School of Electrical and Electronic Engineering, RR@NTU Corp. Lab, Nanyang Technological University, Singapore 639798

*Corresponding author: Tel.: +65-83133542, E-mail address: assel001@e.ntu.edu.sg

Highlights

- Heat transfer performance comparison between finned and pin-fin heat sink
- Laminar and turbulent flow with air and fuel coolants are considered
- Pin-fin double reduce the heat sink weight
- Pin-fins heat sink is almost double overcomes the thermal performance of finned shape

Abstract

This study investigates the heat transfer performance of finned and pin-fin heat sinks for high power density converter in future aircraft. There is a lack of studies evaluating the cooling performance of pin-fin as compared to the finned heat sink configuration. The influence of the aspects such as type of fluid flow (laminar or turbulent), type of working fluid (fuel or air) and geometry configuration (pin-fin or finned shaped heat sink) on heat transfer performance is compared. Circular, cone and hydrofoil pin fin arrays are considered. It is concluded that the thermal performance of pin-fin heat sink is superior to the finned configuration by 1.6-2 times in all cases except when fuel coolant is employed at turbulent flow. As weight of heat sink is concerned, the use of pin-fin shape can reduce half the weight of heat sink. The results of this paper are the guidance which can be applied while designing the heat sink for power electronics in future aircraft.

Nomenclature

A	area (m^2)
c_p	specific heat (J/kg·K)
D_h	hydraulic diameter (m)
h	heat transfer coefficient (W/Km^2)
H	height (m)
k	thermal conductivity (W/Km)
L	length (m)
N	number of channels
Nu	Nusselt number
Δp	pressure drop (Pa)
P_{pump}	pumping power (W)
q	heat flux (W/cm^2)
Re	Reynolds number
T	temperature (K)
U	velocity vector (m/s)
u, v, w	flow velocity (m/s)
W	width (m)
x, y, z	Cartesian coordinates

Greek symbols

μ	viscosity ($N·s/m^2$)
ρ	density (kg/m^3)

Subscripts

j	junction
in	inlet
out	outlet

1. Introduction

More electric engine (MEE) is a trend in aircraft sector. MEE technology is implemented by replacing the mechanical load by the electrical one. This leads to the improvement such as fuel efficiency, reliability and reduction in operation cost. The electric loads is supplied from power buses by using power converter to interface them. Thus, power converter with emphasis on weight reduction and size minimization becomes essential. And cooling system of power converter becomes the main challenge. Some studies on power converter cooling system technology are available in literature [1]. This work discussed the availability of working coolant on aircraft and the capability to meet the cooling requirements by taking into the account the weight and size of the heat sink.

Pin fin heat sink seems to be promising for aircraft cooling system. The latest work of the same group [2] deal with the heat transfer enhancement by applying the perforated pin fin heat sink for cooling system in future aircraft. It is concluded that perforation can not only improve the heat transfer but also results in weight reduction.

Another prospective way to improve heat transfer could be simply change the shape of pin fin arrays as some of the studies are reported. Hua et al [3] experimentally investigated thermal performance of micro pin fin heat sinks with circular, ellipse, diamond, square and triangle pin fin shape. They realized that the effect of shape and size of pin fin increases with Reynolds number. A parametric performance evaluation study by employing five micro pin fin heat sinks with different spacing, arrangements and shapes is conducted experimentally by Koşar and Peles [4]. They concluded that utilizing streamlined pin fin heat sinks can essentially improve the thermal hydraulic performance at the Reynolds number ranging from 14 to 720. Same authors investigated the heat transfer, boiling inception and pressure drop over a bank of micro pin fins in theirs early work [5]. A new correlation is developed to predict the experimental data of water and R-123. Izci et al. [6] numerically investigated the micro pin-fin shape on thermal and hydraulic performance of micro pin-fin heat sinks. Seven shapes of heat sinks were considered, the cone-shaped pin-fin configuration is the preferable choice among all due to the best thermal performance index. Hasan [7] numerically investigated the flow and heat transfer characteristics in micro pin fin heat sink by applying nanofluid as the coolant. The author concluded that circular fins give the highest heat transfer rate as compared to the square, triangular and unfinned heat sink. Numerical studies on optimizing micro square pin-fins heat sink is done by Zhao et al. [8]. They have found the optimal porosity and located angle for better thermal performance. The benefit if using strip, square and circular pin fins is studied numerically by Al-Sallami et al [9]. Based on detailed investigation, strip fins are the most effective thanks to the combined effect of increased wetted surface area and increased turbulence. Heat transfer performance of pin fins with the Reynolds number ranging from 60 to 800 is studied experimentally by Liu et al. [10]. New correlation for the average Nusselt number is proposed. Thermal and hydraulic performance of micro pin-fins heat sinks with circular and square pin-fins structures is studied by John et al. [11]. They investigated the effect of aspect ratio and hydraulic diameter of the pins as well as compared circular and square pin fins based on FOM (a figure of merit). It's concluded that the selection if a pin-fin structure depends on the range of Reynolds number. Performance enhancement of straight and wavy channel heat sink with pin fins is studied by Khoshvaght -Aliabadi et al. [12]. They concluded that pin fin interruption has a considerable effect on the heat transfer improvement both in straight and wavy channel. Yang et al. [13] is investigated the heat removal capacity in microchannel heat sink with rhombus, hydrofoil and sine type of pin fins in laminar flow. They concluded that flow of sine pin fin is more uniform that results in the best heat transfer performance as well as the lowest pressure drop. Duangthongsuk and Wongwises [14] reported an experimental investigation on thermal performance and pressure drop in circular and square pin fin applying SiO_2 nanofluid as a coolant. The studies concluded that the performance of circular pin fin is better than square by about 6-9%. Ramphueiphad and Bureerat [15] demonstrated the multiobjective optimization of pin fin heat sink with several pin fin cross-sections. The study drew the conclusion that the new type of heat sink overcomes the performance of the traditional one.

Finned heat sink is an alternative to pin fin heat sink. Finned heat sink with different geometric structures is compared with the conventional rectangular microchannel by Xia et al. [16]. They came to the point that rectangular head shape provides the better flow velocity uniformity than the trapezoidal headers. Forced convection heat transfer is studied in rectangular finned microchannel heat sink with non-Newtonian nanofluids by [17] using two-phase mixture model. Numerical study of thermal enhancement in microchannel heat sink with secondary flow is presented by Kuppusamy et al. [18]. Overall they concluded that secondary passage in finned microchannel enhances the thermal performance greatly. Only few studies have compared the performance between pin-fin with finned shape heat sink. Jasperson et al. [19] compared micro-pin-fin and microchannel heat sink based on the thermal-hydraulic performance and manufacturability. They concluded, micro-pin-fin heat sinks are roughly three times expensive to fabricate.

This study investigates three-dimensional conjugate heat transfer of finned and pin-fin heat sinks for 50kW high power density converter for future aircraft. The main purpose of this research is to find the most promising heat sink geometry configuration by assuming the available coolants on aircraft. Liquid (fuel) and air coolants at laminar and turbulent with inlet velocity of 70C are considered. The code is validated with available experimental results.

2. Numerical Method

Fig. 1 shows the 50-kW three-phase two-level power converter under analysis, structure of power module and Fig. 2 the schematic diagram of a heat sinks with finned, circular, cone and hydrofoil pin-fins shape. The detailed parameters of the module are listed in Table I. The dimensions of the module are presented in Table I. The $L \times W$ size of heat sink fits three CAS120M12BM2 1.2kV, 120A silicon carbide half-bridge power modules [20]. The gap between power modules is 2 mm and the inlet coolant is defined with a uniform temperature of 70°C and the flow is assumed to reach the atmospheric pressure at the outlet. The liquid type (fuel) and air are considered in this study. All pin fins have the diameter of 3mm and height of 7mm. Hydrofoil shape has the conic arc with shape parameter of 0.5. Thermo-physical properties of fuel and air is taken from [2]. The inlet velocity for each type of flow is presented in Table 2. In this paper the combined effect of flow regime and type of coolant is divided into four cases in order to find an appropriated type of heat sink in each case.

Case 1: Laminar flow and air coolant
Case 2: Turbulent flow and air coolant
Case 3: Laminar flow and liquid coolant
Case 4: Turbulent flow and liquid coolant

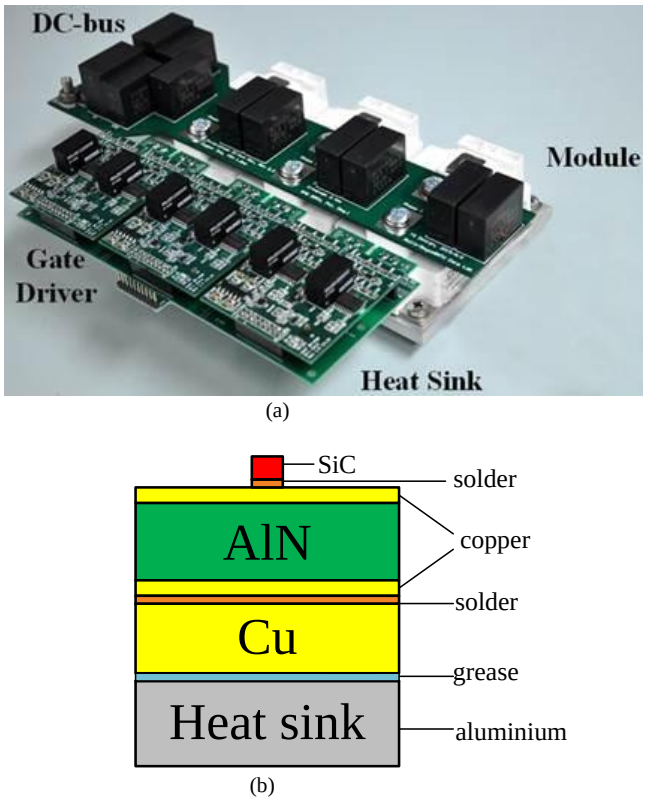

Fig. 1. (a) 50-kW power converter, (b) structure of power module

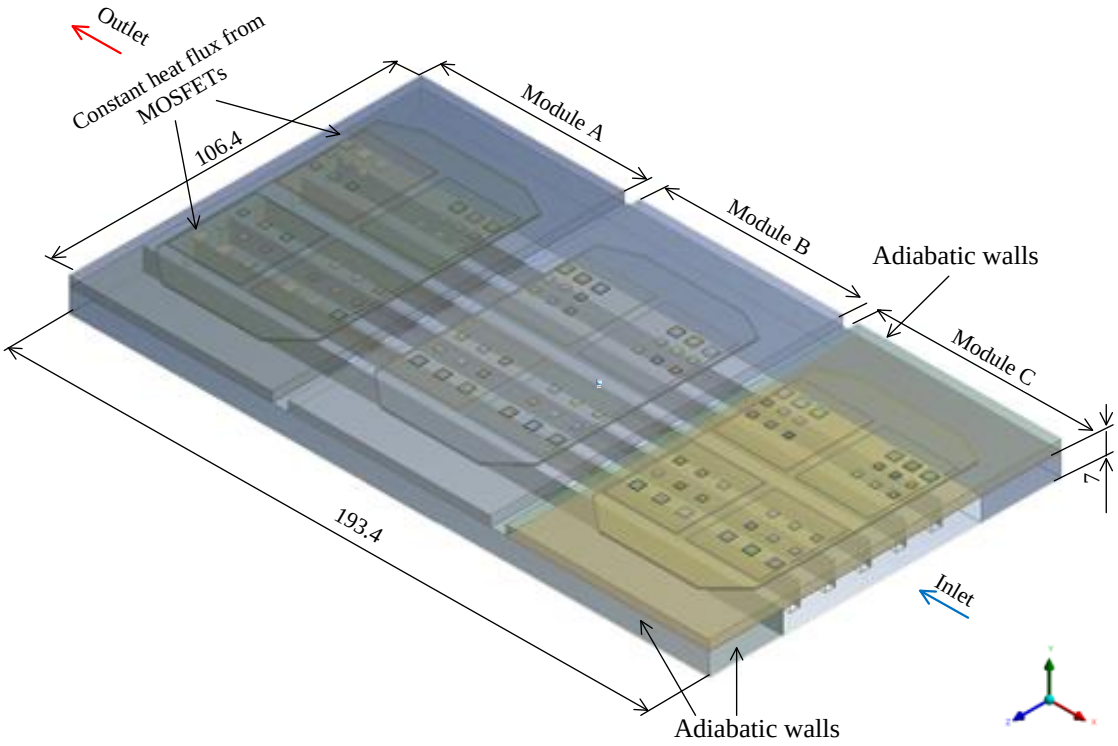
Outlet
Constant heat flux from MOSFETs
106.4
Module A
Module B
Adiabatic walls
Module C
7
193.4
Inlet
Adiabatic walls

(a)

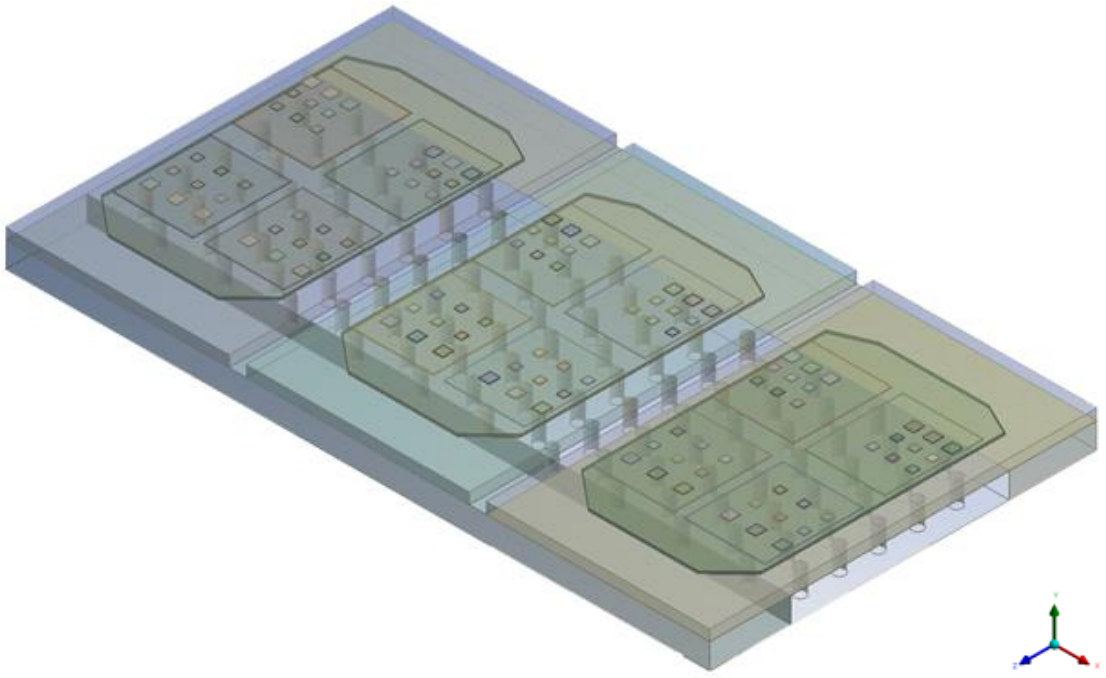

(b)

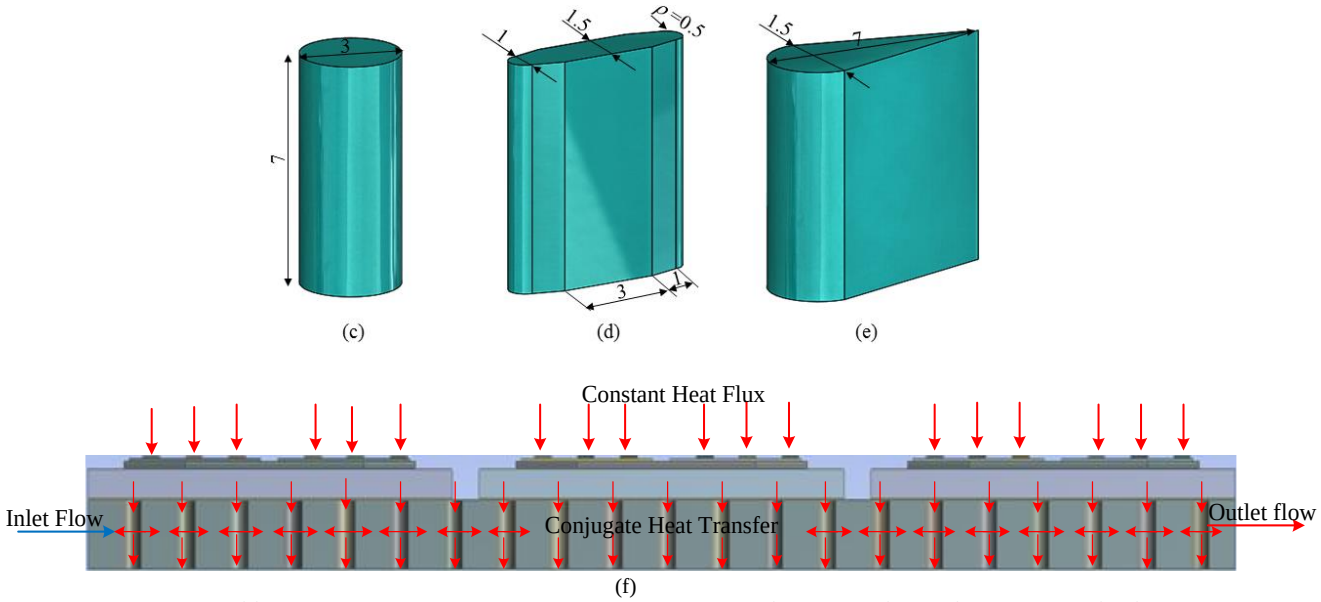

Fig. 2. (a) The diagram of finned heat sink (b) circular shape heat sink, (c) circular pin-fin, (d) hydrofoil pin-fin, (e) cone pin-fin (f) conjugate heat transfer

Table 1. Height and material properties of the module

Name	Thermal conductivity (W/mK)	Height (mm)
SiC	120	0.18
Solder	58.7	0.15
Copper (DBC)	387.6	0.3
AlN	150	0.3
Thermal grease	5	0.1
Aluminum	170	7
Copper (pins)	387.6	6

Table 2. Working coolant and inlet velocity

Coolant	Velocity, m/s	
	Turbulent flow	Laminar flow
fuel	1 - 5	0.01-0.05
air	4 - 8	1 - 3

The boundary conditions are listed as below:

Channel inlet:

$$u = u_{in},\ \ v = 0,\ \ w = 0,\ T = T_{in} \tag{1}$$

Channel outlet:

$$p = p_{out} \tag{2}$$

Coolant – solid interface:

$$u = v = \omega = 0,\ \ T_f = T_s,\ -k_f \frac{\partial T_f}{\partial n} = -k_s \frac{\partial T_s}{\partial n} \tag{3}$$

Bottom wall of the heat sink:

$$q_w = -k_s \frac{\partial T_s}{\partial n} \tag{4}$$

Other solid walls and symmetric boundaries:

$$-k_s \frac{\partial T_s}{\partial n} = 0 \tag{5}$$

The following assumptions are taken to simplify the analysis:

- single-phase, incompressible laminar (oil) and turbulent flow (water, fuel, oil);
- negligible effect of gravitational force and heat dissipation caused by viscosity and
- natural convection and radiation are neglected

Under these simplifications, 3D steady governing equations for the conjugate heat transfer can be written as follows [21]:

Continuity equation

$$\frac{\partial u}{\partial x}+\frac{\partial \nu}{\partial y}+\frac{\partial w}{\partial z}=0 \tag{6}$$

Momentum equation

$$\rho_f\left(u\frac{\partial u}{\partial x}+\nu\frac{\partial u}{\partial y}+w\frac{\partial w}{\partial z}\right)=-\frac{\partial P}{\partial x}+\mu_f\left(\frac{\partial^2 u}{\partial x^2}+\frac{\partial^2 u}{\partial y^2}+\frac{\partial^2 u}{\partial z^2}\right) \tag{7}$$

$$\rho_f\left(u\frac{\partial \nu}{\partial x}+\nu\frac{\partial \nu}{\partial y}+w\frac{\partial \nu}{\partial z}\right)=-\frac{\partial P}{\partial y}+\mu_f\left(\frac{\partial^2 \nu}{\partial x^2}+\frac{\partial^2 \nu}{\partial y^2}+\frac{\partial^2 \nu}{\partial z^2}\right) \tag{8}$$

$$\rho_f\left(u\frac{\partial w}{\partial x}+\nu\frac{\partial w}{\partial y}+w\frac{\partial w}{\partial z}\right)=-\frac{\partial P}{\partial z}+\mu_f\left(\frac{\partial^2 w}{\partial x^2}+\frac{\partial^2 w}{\partial y^2}+\frac{\partial^2 w}{\partial z^2}\right) \tag{9}$$

Energy equation for the coolant

$$\rho_f c_{p.f}\left(u\frac{\partial T_f}{\partial x}+\nu\frac{\partial T_f}{\partial y}+w\frac{\partial T_f}{\partial z}\right)=k_f\left(\frac{\partial^2 T_f}{\partial x^2}+\frac{\partial^2 T_f}{\partial y^2}+\frac{\partial^2 T_f}{\partial z^2}\right) \tag{10}$$

Energy equation for the solid region

$$0=k_s\left(\frac{\partial^2 T_s}{\partial x^2}+\frac{\partial^2 T_s}{\partial y^2}+\frac{\partial^2 T_s}{\partial z^2}\right) \tag{11}$$

Turbulent kinetic energy

$$\frac{\partial(\rho k)}{\partial t}+\frac{\partial(\rho u_j k)}{\partial x_j}=P-\beta^*\rho k\omega+\frac{\partial}{\partial x_j}\left[(\mu+\sigma_k\mu_t)\frac{\partial k}{\partial x_j}\right] \tag{12}$$

where P is a production limiter, $P=\tau_{ij}\dfrac{\partial u_i}{\partial x_j}$

Specific dissipation rate

$$\frac{\partial(\rho\omega)}{\partial t}+\frac{\partial(\rho u_j\omega)}{\partial x_j}=\frac{\gamma}{\nu_t}P-\beta\rho\omega^2+\frac{\partial}{\partial x_j}\left[(\mu+\sigma_\omega\mu_t)\frac{\partial\omega}{\partial x_j}\right]+2(1-F_1)\frac{\rho\sigma_{\omega 2}}{\omega}\frac{\partial k}{\partial x_j}\frac{\partial\omega}{\partial x_j} \tag{13}$$

where the blending function F_1 is defined by

$$F_1=\tanh\left\{\left\{\min\left[\max\left(\frac{\sqrt{k}}{\beta^*\omega y},\frac{500\nu}{y^2\omega}\right),\frac{4\rho\sigma_{\omega 2}k}{CD_{k\omega}y^2}\right]\right\}^4\right\} \tag{14}$$

With $CD=\max\left(2\rho\sigma_{\omega 2}\dfrac{1}{\omega}\dfrac{\partial k}{\partial x_i}\dfrac{\partial\omega}{\partial x_i},10^{-10}\right)$ and y is the distance to the nearest wall.

And the turbulent eddy viscosity is computed from

$$\mu_t = \frac{\rho \alpha_1 k}{\max(\alpha_1 \omega, SF_2)} \tag{15}$$

where S is the invariant measure of the strain rate and F_2 is second blending function
The constants are: β^*=0.09, α_1=5/9, $\sigma_{\omega 2}$=0.856,σ_{k1}=0.85, σ_{k2}=1, σ_k and σ_ω are the turbulent Prandtl numbers for k and ω respectively.

Based on ANSYS Fluent R17.0, the 3D conjugate heat transfer problem is numerically solved. Implicit solver option is used to solve the governing equations. The second order upwind scheme is adopted for both energy and momentum discretization, while for pressure discretization a standard interpolation scheme is adopted. The pressure-velocity coupling is implemented by SIMPLE algorithm. The convergence criteria for the x, y, and z directions velocity are set to 10^{-6} while the residuals of energy equations are restricted to 10^{-7}.

Thermal resistance is defined as

$$R_{th} = \frac{T_j - T_{in}}{qA} \tag{16}$$

where T_j is the junction temperature, T_{in} is the inlet temperature of the coolant, and qA is the heat flow.

Pump power is defined as

$$P_{pump} = \Delta p \cdot \dot{V} \tag{17}$$

where Δp is the pressure drop between inlet and outlet of the heat sink, V Is the volumetric flow rate of the coolant.

Convective heat transfer coefficient and Nusselt number are determined as

$$h = \frac{Q}{A_s[T_w - (\frac{T_{out} + T_{in}}{2})]} \tag{18}$$

where A_s is the surface are of the heat sink, T_w is the base plate temperature, K

$$Nu = \frac{hD_h}{k} \tag{19}$$

Pin fin pressure loss is defined as

$$\Delta P_{fin} = \frac{\int_{Finsurfaces} F_x dA}{A_{fin,sur}} \tag{20}$$

Fin Friction factor is expressed as in [6]

$$f_{fin} = \frac{2(\Delta P_{fin})}{\rho u_{\max}^2} \tag{21}$$

Thermal hydraulic performance index [6] is the ratio of heat transfer improvement to the pump power and defined as

$$\eta = \frac{Nu / Nu_{0P}}{(f / f_{0P})^{1/3}} \tag{22}$$

3. Grid independent study and simulation validation

In order to obtain an appropriate mesh grid, three grid size is compared at air inlet velocity of 6.5m/s and summarized in Table 3. The effect of grid resolution is shown in terms of MOSFET temperature and pressure drop. The difference between mesh 1 and mesh 2 is 1.9 % and 7.5% for MOSFET temperature and pressure drop, respectively. The difference between mesh 2 and mesh 3 is 0.08% and 2.5% for MOSFET temperature and pressure drop, respectively. Mesh 2 is chosen for all cases as the best trade-off between both accuracy and processing time [2]

Table 3. Grid independence study data.

	Number of cells	T (C)	ΔP (kPa)
Mesh 1	5302045	78	43
Mesh 2	3466698	76.5	40
Mesh 3	2327091	76.44	39

Fig. 3 compares the experiment data of [22] with the current simulation results in a case of maximum MOSFET temperature and pressure drop with the same grid size as in [22] for circular pin fin (0P) and circular pin fin with three perforations (3P). *k-ω SST* and *k-ε* with enhanced wall treatment as turbulent models are compared. The inflation layer is generated near the walls in order to capture the boundary layers. The $y+ \leq 3$ and the $y+$ value is on the order of 1 to 1.8. The number of layers is 20. These mesh requirements are applied for both turbulent models as they have similar near-wall requirements. Both turbulent models are good coincides with [22] with maximum discrepancy of 10%. Same as in [22] *k-ω SST* model is chosen for current study.

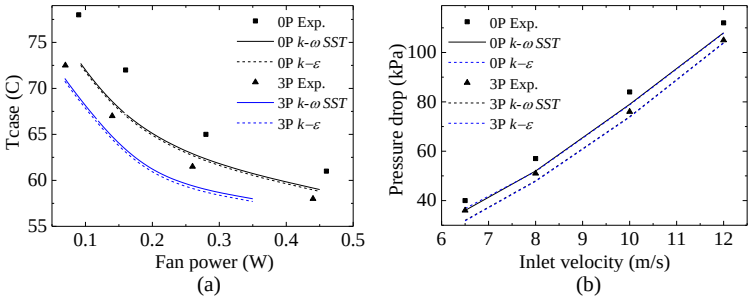

Fig. 3. Comparison between experimental and numerical prediction when (a) T_{case} is a function of fan power (b) pressure drop is a function of airflow speed

4. Results and discussion

4.1 Case 1: Finned and pin-fin heat sink comparison at laminar flow with air coolant

Fig. 4 shows the velocity vectors circular, cone and hydrofoil of pin fin heat sinks when air is applied as a coolant at low *Re* number (laminar flow) (*Re*=595-1785). Overall for all types of heat sinks the flow separation occurs due to fins. Flow separation causes the wake formation. The length and width of the wake behind is bigger for circular and cone rather than for hydrofoil shape owing to the hydrofoil streamlined shape. The hydrofoil streamlined shape is designed in such a way that surface creates the least disturbance in the air flow, produces the lowest resistance and lowers the friction drag. In addition, the streamlines of circular and cone pin-fins take the sinusoidal form while they are more straight lines for the hydrofoil.

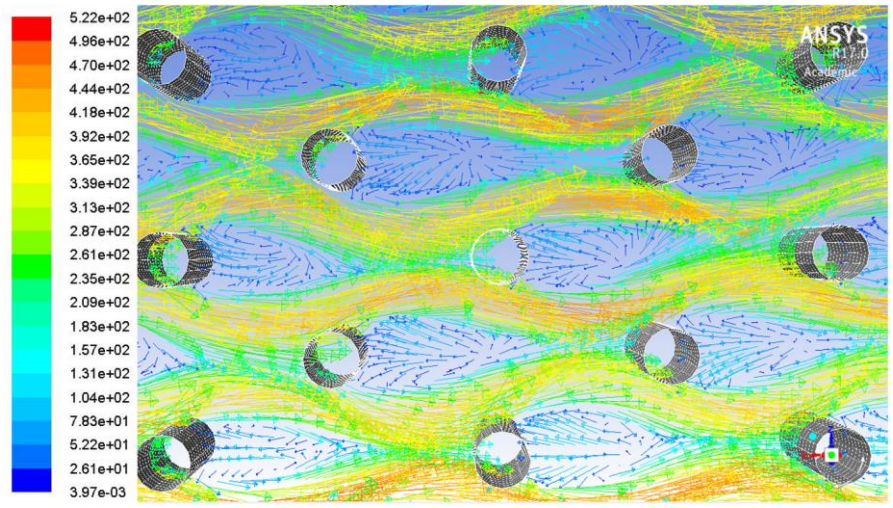

(a)

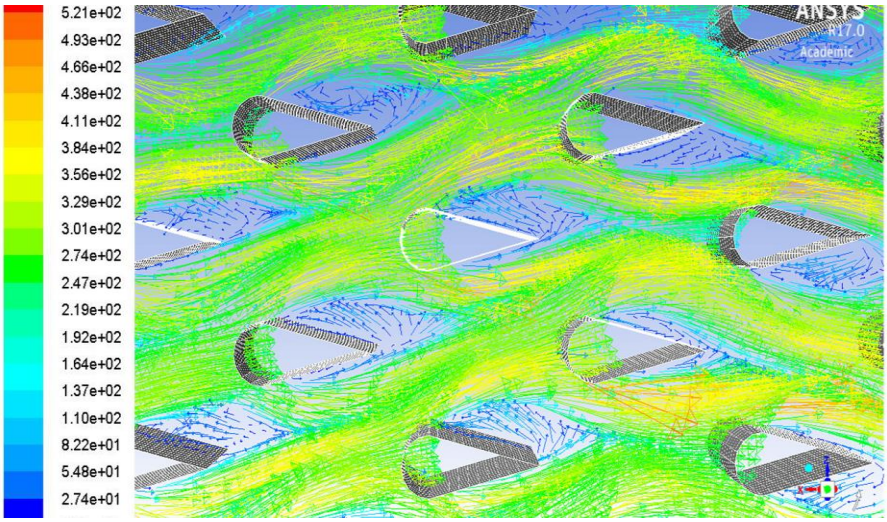

(b)

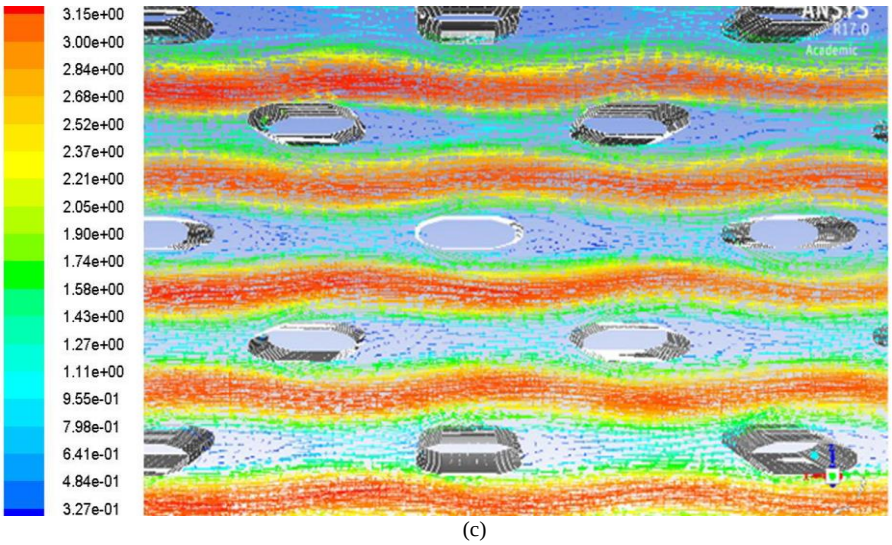

(c)

Fig. 4. Velocity vectors of (a) circular, (b) cone and (c) hydrofoil pin-fin heat sink

Fig. 5 shows the heat transfer coefficient, *h* and Nusselt number, *Nu* for various types of pin fin heat sinks which has the same trends. It's common for all, *h* and *Nu* increases with *u*. Cone pin fin has the highest *h* and *Nu* over the all inlet velocity range followed by circle, hydrofoil and finned shapes. The difference between circular, cone and hydrofoil with finned shape in terms of *h* and *Nu* of cone increases with *u*. The pin fin shapes outperform the finned shape which could be explained as follows. The pin fins trigger the separation effects which leads to the better air mixing and heat transfer increase. The similar observations is obtained by [6].

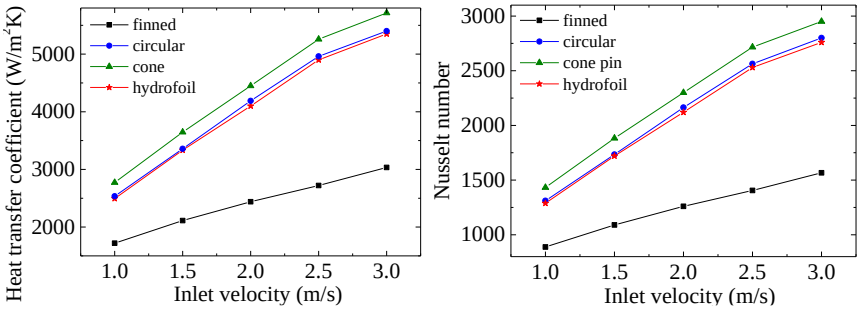

Fig. 5. Heat transfer coefficient and Nusselt number

Fig. 6 demonstrates friction factor, *f* as a function of inlet velocity. It can be noticed that circular and cone shapes have the highest *f* and the difference between them and the rest of the pin-fin configurations in term of *f* is keep increasing with *u*. The highest *f* of circular and cone shapes could be explained as follows. A moving fluid experiences a drag force which is the combined effect of friction drag and pressure drag. Friction drag (or skin friction) caused by the friction between the fluid and body surface. It associates with the development of boundary layers. And pressure drag is proportional to the pressure difference between front and back area of the immersed body. The pressure drag is also called form drag since it strongly depends on the body shape. If the drag force is dominated by the friction drag then the body can be considered as streamlined. The larger surface area the larger friction drag will be since the friction drag is proportional to the surface area. The pressure drag is dominant for blunt bodies. When a fluids passing over the blunt body at high velocity the recirculating happens and back flows happen which is called separation region. The larger separation region the larger pressure drag occurs. And area of the separation region decreases with velocity reduction. The hydrofoil shaped pin can be considered as streamlined body and the viscous drag is dominated in this case. Circular shape pins are considered blunt bodies since the drag is dominated by pressure drag. However the pressure drag in circular shaped pin is much more noticeable as compared to the viscous drag in hydrofoil shaped pin.

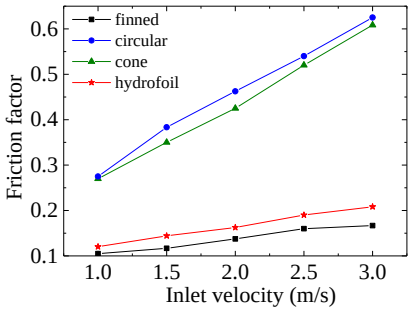

Fig. 6. Friction factor versus inlet velocity

Fig. 7 shows the thermal resistance, R_{th} as a function of pump power and thermal performance index as a function of *u*. For a given pump power input, the hydrofoil shapes is able to provide the lowest R_{th} followed by cone, circle and finned shapes. This coincides with the thermal performance index sequence where the worst case such a finned shape is taken as a reference. Hydrofoil shape has the sharp decrease with pump power which results in more noticeable thermal performance index increase with *u*. However at the *u* = 2.5-3m/s it starts to saturate. The highest thermal performance index for hydrofoil shape is 1.7. The trend for circular and cone shapes is similar. Initially R_{th} decreases significantly and slowly reaches the saturation. The highest thermal performance index is noticed at

u = 2.5m/s with the values of thermal performance index of 1.3 and 1.1 for cone and circular shapes accordingly. Thus employing the hydrofoil pin-fin shape in this case is more rational.

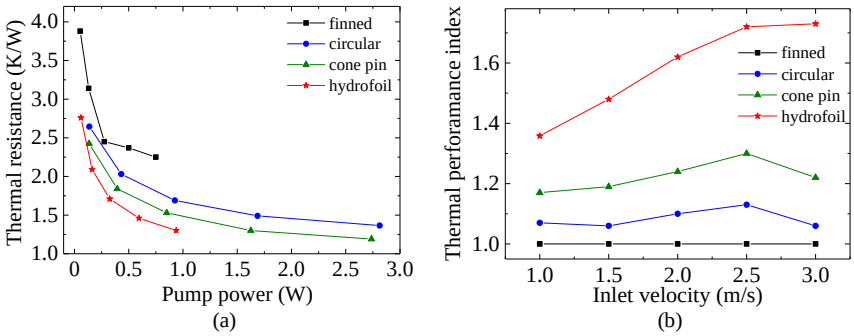

Fig. 7. (a) Thermal resistance versus pump power and (b) thermal performance index versus inlet velocity

4.2 Case 2: Finned and pin-fin heat sink comparison at turbulent flow with air coolant

Fig. 8 shows the velocity vectors of circular, cone and hydrofoil pin fin heat sinks when air is applied as a coolant at high *Re* number (turbulent flow) (*Re*=2380-4761). Circular and cone shaped pin-fin heat sink is experienced the flow separation due to pin-fins which results in flow mixing and wake occurrence. Whereas there is no flow separation in a case of hydrofoil shape. The more pronounced flow separation is noticed for circular shape. However the wake zone of circular and cone shapes in this case is obviously narrow and smaller as compared with the wake formed at low *Re* (laminar flow).

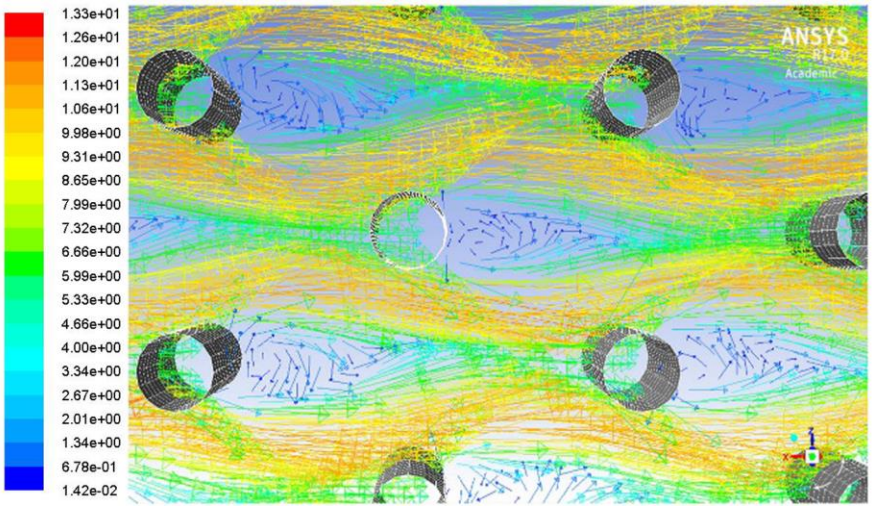

(a)

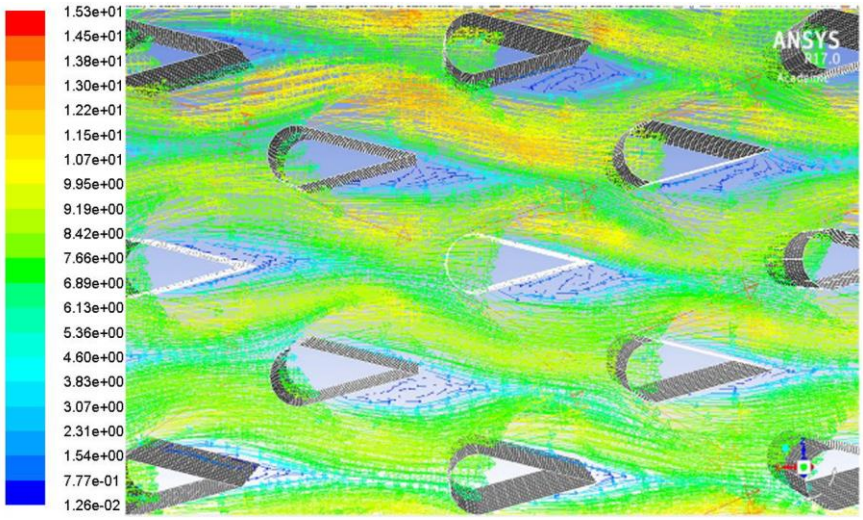

(b)

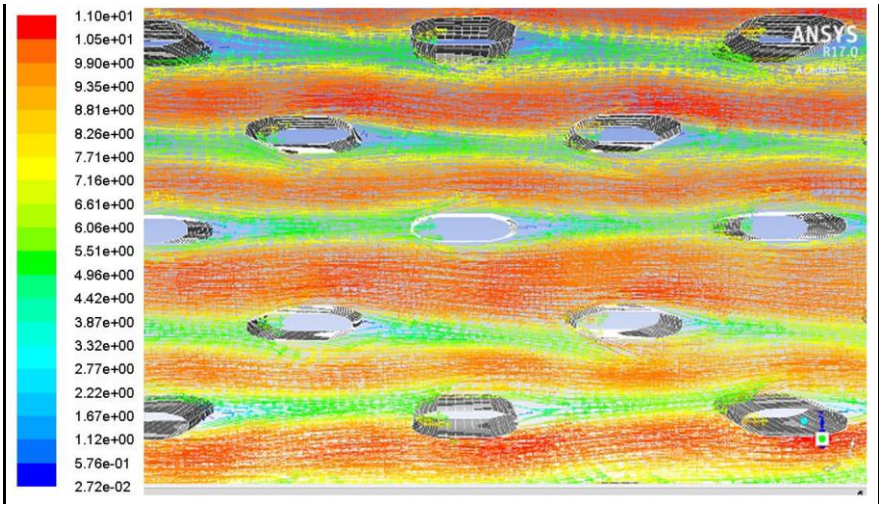

(c)

Fig. 8. Velocity vectors of (a) circular, (b) cone and (c) hydrofoil pin-fin heat sink

Fig. 9 demonstrates *h* and *f* and according to it, finned heat sink results in the lowest *h* followed by circular, hydrofoil and cone shapes. Overall the *h* and *f* increases with *u*. The *h* lines are almost parallel to each other. As far as *f* is concerned, hydrofoil and finned shapes have the same lowest value of *f* at *u* = 4-6m/s while *f* value of finned shape goes up more than hydrofoil one at *u* = 7-8m/s. Circular and cone types of pin-fins have the convex shape which causes the highest *f*. The hydrofoil streamlined shape lowers the friction drag.

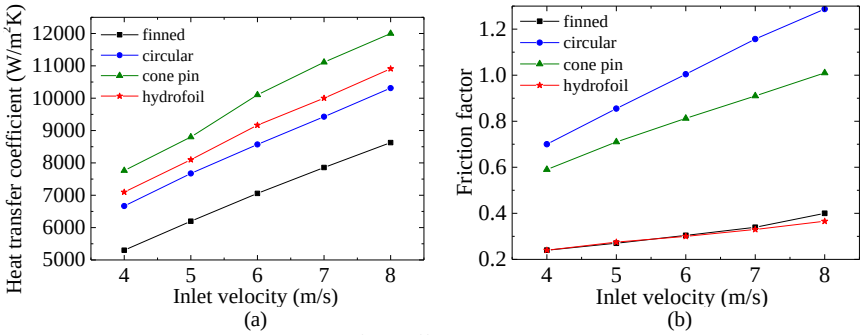

Fig. 9 Heat transfer coefficient and Nusselt number

Fig. 10 shows the R_{th} as a function of pump power and thermal performance index as a function of *u*. It's common for all, R_{th} decreases with pump power. The lowest R_{th} provided by hydrofoil followed by cone, finned and circle pin-fins accordingly. Considering thermal performance index, the circular shape is taken as a reference due to the worst thermal performance. The apparent improvement by employing hydrofoil shape is noticed at *u* = 6m/s. The further increase in *u* does not significantly contributes into thermal performance index value. Thermal performance index of cone shape slowly increases and reaches the saturation point at *u* = 6m/s whereas the remarkable increment in thermal performance index is visible for cone shape at the range of *u* = 4-7m/s and then it goes down. The conclusion of this case is that the hydrofoil shape pin-fin is the most prominent heat sink configuration.

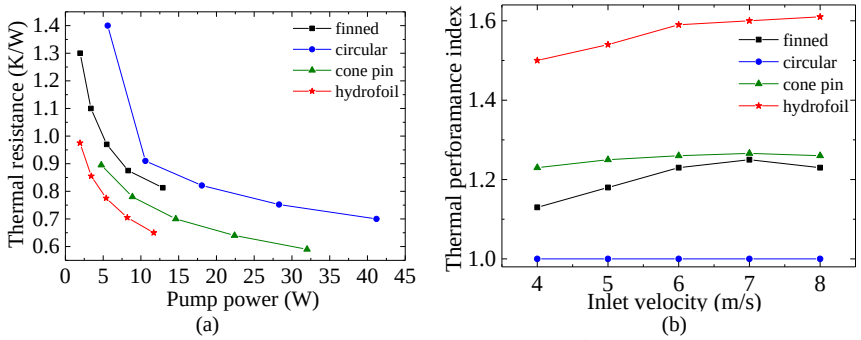

Fig. 10. (a) Thermal resistance versus pump power and (b) thermal performance index versus inlet velocity

4.3 Case 3: Finned and pin-fin heat sink comparison at laminar flow with fuel coolant

Fig. 11 shows the velocity vectors circular, cone and hydrofoil pin-fin heat sinks when fuel is applied as a coolant at low *Re* number (laminar flow) (*Re*=312-1562). The flow separation occurs for all types of pin-fin heat sinks causes the wake formation behind the pin-fins. The longest and broadest wake is formed by circular shape followed by cone and hydrofoil. The size of the wake depends on the shape of the pin-fins. The more streamlined shape is the smaller the size of the wake.

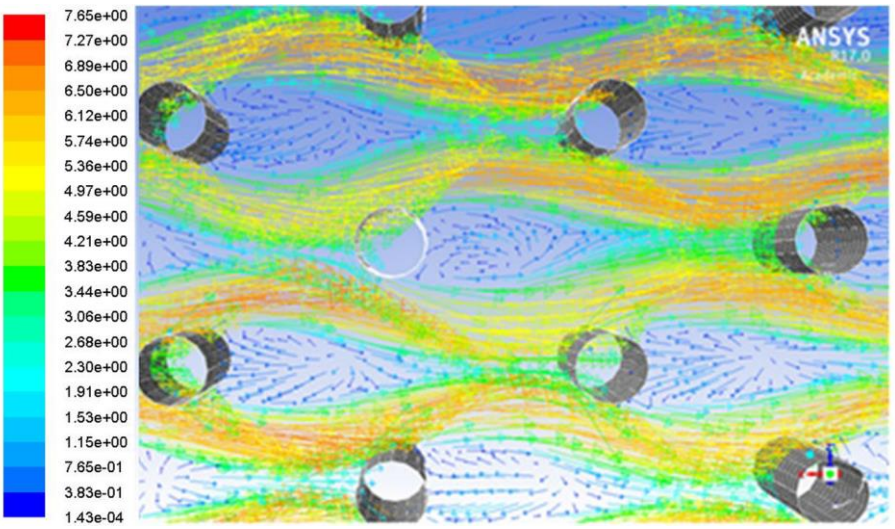

(a)

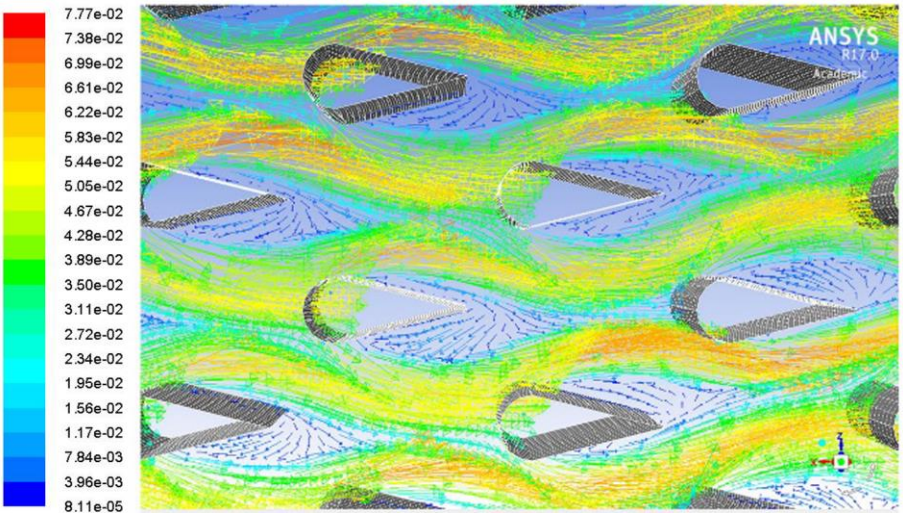

(b)

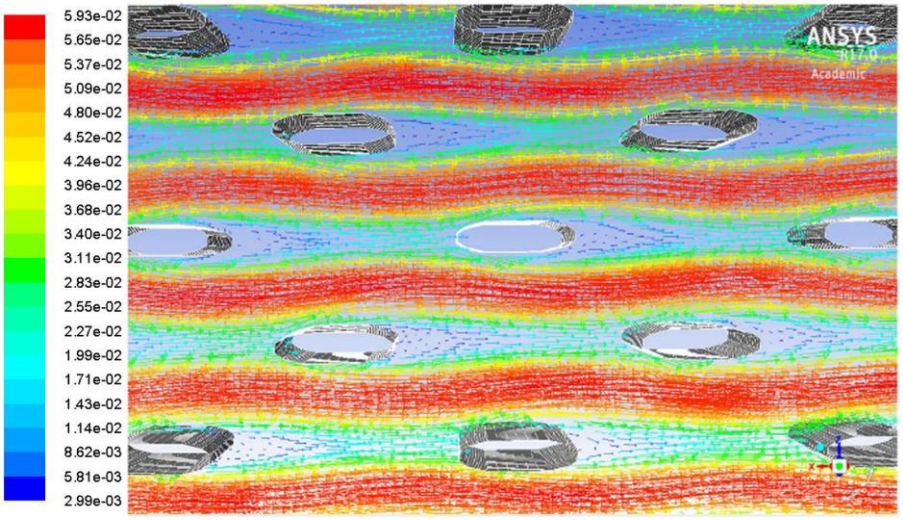

(c)

Fig. 11. Velocity vectors of (a) circular, (b) cone and (c) hydrofoil pin-fin heat sink

Fig. 12 presents the relationship between u and h. Overall h increases with u. However in the case of finned, hydrofoil and circular shape h increases twice at the range of u = 0.01-0.05m/s whereas for cone shape h increment is about 2.5 times. The highest h is obtained by cone shape followed by circular, hydrofoil and finned shape. As far as f is concerned, the lowest f is generated by finned followed by hydrofoil, cone and circular shapes accordingly. Again, circular and cone shapes are resulted in prominent f increase by about 3 times within the range of u = 0.01-0.05m/s while its less than two times f increase for the shapes such as finned and hydrofoil. Fig. 12(c) displays the temperature distributions at vertical plane (YZ) at x=0.215m at u=0.03m/s. Hydrofoil (top) and circular (middle) shaped pin-fins results in the similar peak temperature (392K) and temperature distribution overall. By adopting cone shaped pin-fin heat sink (bottom), the hot spot temperature is noticeably lower than the previous ones with maximum peak of 382K.

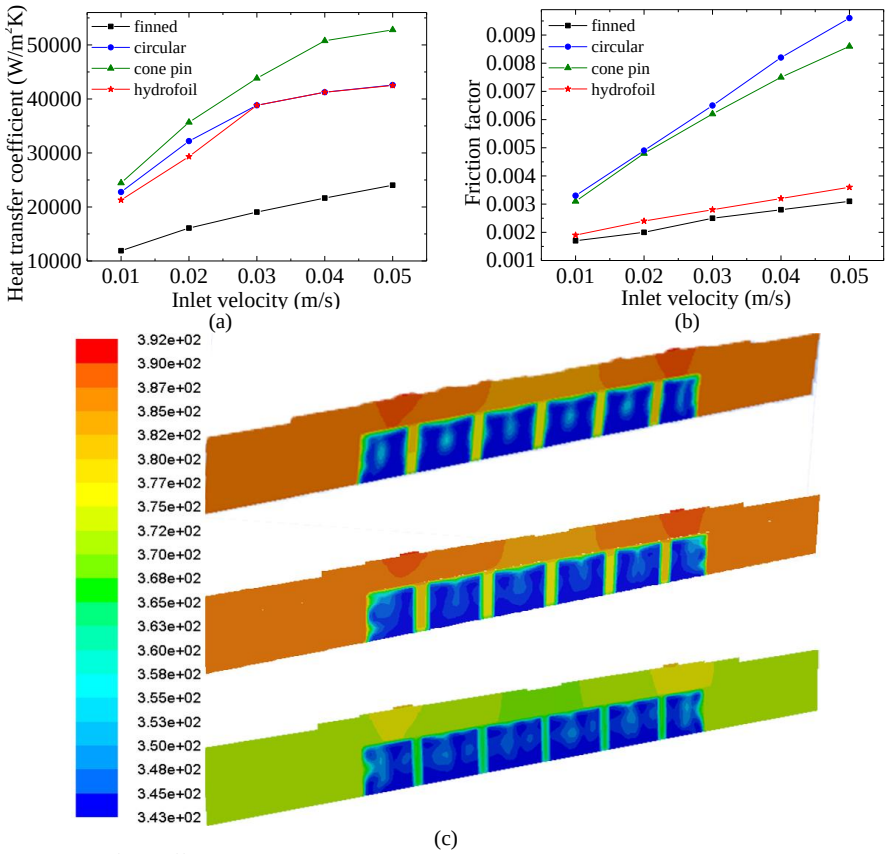

Fig. 12. (a) Heat transfer coefficient, (b) Nusselt number and (c) temperature contours at vertical plane (YZ) at x=0.215m

Pump power versus R_{th} is presented on Fig. 13. The highest R_{th} yields by finned shape which is taken as the reference in Fig. 13(b). The best cooling performance done by cone following by hydrofoil and circular shapes accordingly. For all shapes of pin-fins R_{th} decreases with pump power till u = 0.03m/s. After u = 0.03m/s, circular, cone and hydrofoil shapes slowly reaches the saturation while R_{th} of finned shape still keeps decreasing. That explains the behavior of thermal performance index which reaches the highest value at u = 0.03m/s and significantly decreases right after that. The employment of cone shape is considered the best option in the case of laminar flow with a fuel as a coolant with the highest thermal performance index equal to 2.

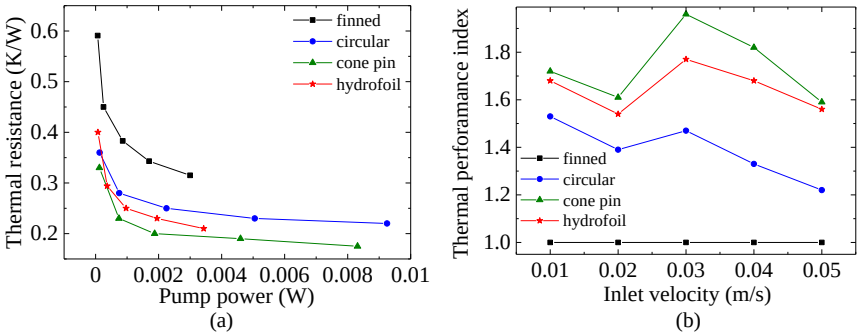

Fig. 13. (a) Thermal resistance versus pump power and (b) thermal performance index versus inlet velocity

4.4 Case 4: Finned and pin-fin heat sink comparison at turbulent flow with fuel coolant

Fig. 14 demonstrates the pin-fin heat sink streamlines at the case of turbulent flow with combination of fuel as the working fluid. The range of inlet velocity is taken for this case is 1-5m/s which corresponds to *Re*=31250-156250. The obvious flow separation is common for circular shape and near the sharp corner for cone shape. While there is no flow separation in a case hydrofoil shape.

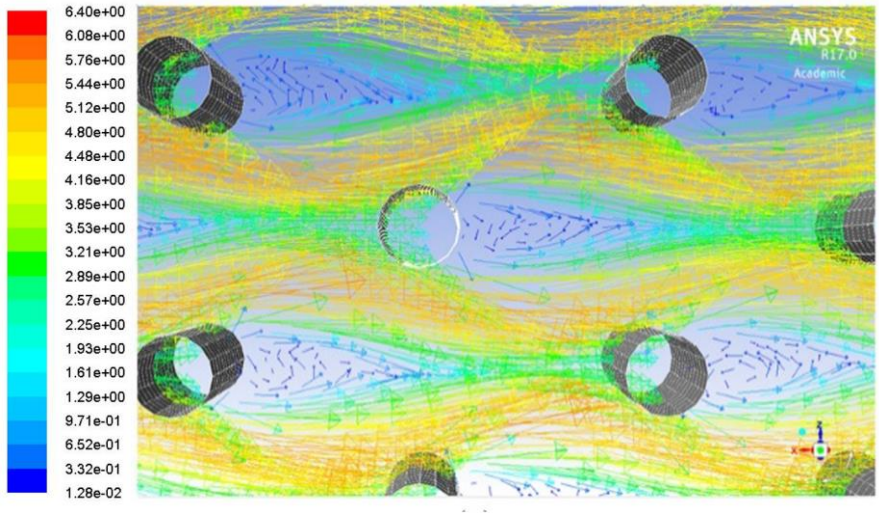

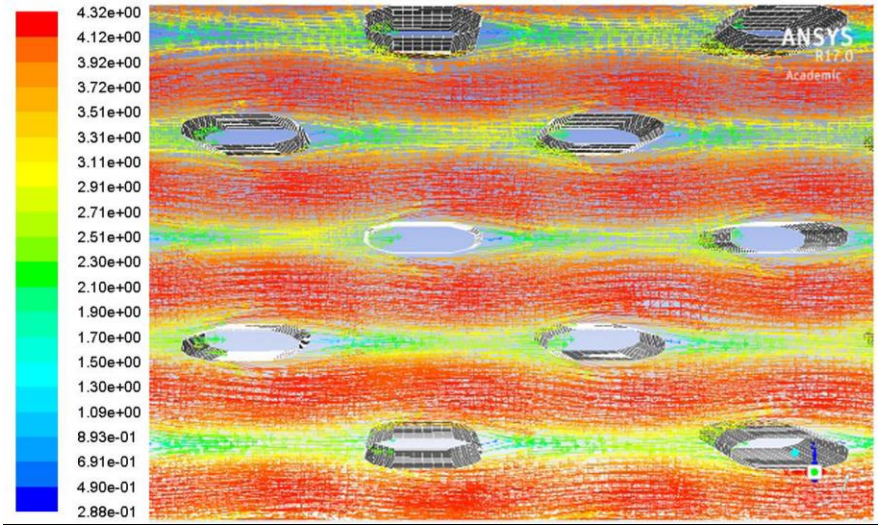

(c)

Fig. 14. Velocity vectors of (a) circular, (b) cone and (c) hydrofoil pin-fin heat sink

Fig. 15(a) represents h in terms of u. The common trend for all the increase of f with u. The highest h exhibits by finned shape. The second highest h provides by cone followed by circular and hydrofoil shapes. There is no visible percentage difference in the value of h with u between all shapes relating to each other. The maximum percentage difference in terms of h between the best and worst results is 7.5%. As far as f is concerned, it significantly increases for each shape by about 5 times within the range of u = 1-5m/s.

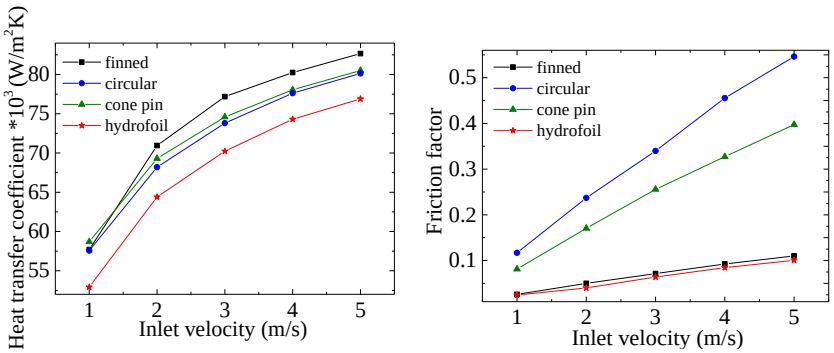

Fig. 15. Heat transfer coefficient and Nusselt number

According to the Fig. 16 the lowest R_{th} versus pump power is provided by finned following by hydrofoil, cone and circular shapes accordingly. The significant R_{th} decrease of finned and hydrofoil shapes is noticed at u = 1-3m/s with regard to the circular shapes which is taken as the reference at Fig. 16(b). After u=3m/s there is no visible decrease in R_{th} as compared to the reference. When it comes to the cone shape, R_{th} decrement is less than that of circular at u = 1-3m/s and almost the same at u = 3-5m/s. This explains the thermal performance decrement first and the constant value right after that. The prominent results are shown by finned shape with the lowest R_{th} and highest thermal performance index.

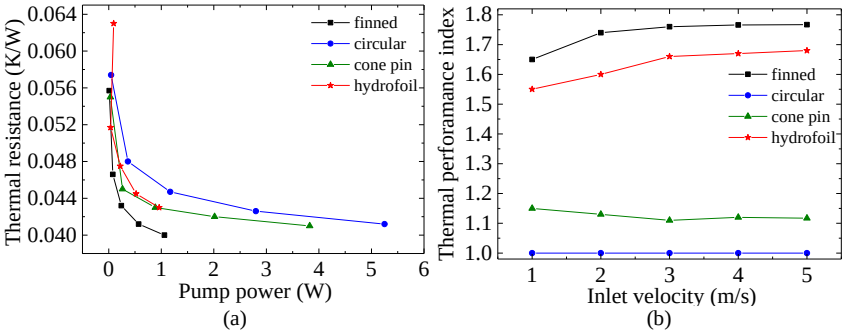

Fig. 16. (a) Thermal resistance versus pump power and (b) thermal performance index versus inlet velocity

The comparison results on heat transfer performance between pin-fin and finned heat sink are summarized in Table 3. Overall pin-fin heat sink is dominant in most of the cases expect at turbulent flow with fuel coolant combination. Thermal performance index is compared in this table in each case as regards to the worst case performance. For example, laminar flow and fuel coolant combination is compared to the finned shape heat sink.

Table 3 Fluid flow and geometry combination results.

	Dominant geometry		Thermal performance index, %	
Coolant/Flow	laminar	turbulent	laminar	turbulent
Fuel	cone	finned	2	1.8
Air	hydrofoil	hydrofoil	1.7	1.6

4.5 Weight consideration

Weight reduction is one of the main concern in aerospace and one of the target of this study. Table 4 shows the data of volume and weight of pin-fin and finned heat sink. Moreover the last column indicates the weight reduction of pin-fin configuration as compared to finned heat sink. In this study, the usage of pin-fin helps to decrease the weight of heat sink at least by half.

Table 4 Pin-fin and finned heat sink weight

	Volume, m^3	Number of fins	Material density (copper), kg/m^3	Weight, kg	Weight reduction, %
Finned	$17.2*10^{-6}$	5	8960	0.17	
Circular	$4.95*10^{-8}$	115	8960	0.05	71
Hydrofoil	$5.37*10^{-8}$	115	8960	0.06	65
Cone	$8.77*10^{-8}$	115	8960	0.09	47

5. Conclusion

This study numerically investigated the heat transfer performance of pin-fin heat sink with circular, cone and hydrofoil fin arrays for high power density converter under aerospace conditions. By aerospace conditions means the employment the available working agents such fuel, oil and air. The simulation data is compared with that of experimental to prove the accuracy of the numerical method. The pin-fin heat sink cooling performance is then compared with the finned heat sink based on heat transfer coefficient, Nusselt number, friction number, thermal resistance and thermal performance index. Pin-fin and finned shapes heat sink is compared at laminar and turbulent flow considering liquid (fuel) and air type as working coolants. Based on simulation results, the following statements are concluded:

- The highest h in Case 1, 2 and 3 is provided by the cone pin-fin heat sink. It is due to flow separation effect caused by pin-fins which lead to the better mixing flow and increase heat transfer.
- The lowest f and Δp are provided by hydrofoil and finned heat sinks due to no flow separation and smaller surface area
- Pin-fin shape overcomes finned shape in terms of thermal performance index in the Cases 1, 2 and 3 by about 1.6 – 2 times.

- Finned heat sink is recommended to be used at turbulent flow with liquid coolant.
- Pin-fins reduces the weight of heat sink to half.

Acknowledgement

This study was conducted within the Rolls-Royce@NTU Corporate Lab with support from the National Research Foundation (NRF) Singapore under the Corp Lab@University Scheme.

Reference

[1] A. Nawawi *et al.*, "Design and Demonstration of High Power Density Inverter for Aircraft Applications," *IEEE Transactions on Industry Applications,* vol. 53, no. 2, pp. 1168-1176, 2017.

[2] A. Sakanova, "Heat transfer enhancement of perforated pin heat sink in future aircraft applications," *Applied Thermal Engineering,* vol. 124, pp. 315-326, 2017/09/01/ 2017.

[3] J. Hua, G. Li, X. Zhao, and Q. Li, "Experimental study on thermal performance of micro pin fin heat sinks with various shapes," *Heat and Mass Transfer,* journal article vol. 53, no. 3, pp. 1093-1104, March 01 2017.

[4] A. Kosar and Y. Peles, "TCPT-2006-096.R2: Micro Scale pin fin Heat Sinks —Parametric Performance Evaluation Study," *IEEE Transactions on Components and Packaging Technologies,* vol. 30, no. 4, pp. 855-865, 2007.

[5] A. Koşar and Y. Peles, "Convective flow of refrigerant (R-123) across a bank of micro pin fins," *International Journal of Heat and Mass Transfer,* vol. 49, no. 17–18, pp. 3142-3155, 8// 2006.

[6] T. İzci, M. Koz, and A. Koşar, "The Effect of Micro Pin-Fin Shape on Thermal and Hydraulic Performance of Micro Pin-Fin Heat Sinks," *Heat Transfer Engineering,* Article vol. 36, no. 17, pp. 1447-1457, 2015.

[7] M. I. Hasan, "Investigation of flow and heat transfer characteristics in micro pin fin heat sink with nanofluid," *Applied Thermal Engineering,* vol. 63, no. 2, pp. 598-607, 2014/02/22/ 2014.

[8] J. Zhao, S. Huang, L. Gong, and Z. Huang, "Numerical study and optimizing on micro square pin-fin heat sink for electronic cooling," *Applied Thermal Engineering,* vol. 93, pp. 1347-1359, 1/25/ 2016.

[9] W. Al-Sallami, A. Al-Damook, and H. M. Thompson, "A numerical investigation of thermal airflows over strip fin heat sinks," *International Communications in Heat and Mass Transfer,* vol. 75, no. Supplement C, pp. 183-191, 2016/07/01/ 2016.

[10] M. Liu, D. Liu, S. Xu, and Y. Chen, "Experimental study on liquid flow and heat transfer in micro square pin fin heat sink," *International Journal of Heat and Mass Transfer,* vol. 54, no. 25–26, pp. 5602-5611, 12// 2011.

[11] T. J. John, B. Mathew, and H. Hegab, "Parametric study on the combined thermal and hydraulic performance of single phase micro pin-fin heat sinks part I: Square and circle geometries," *International Journal of Thermal Sciences,* vol. 49, no. 11, pp. 2177-2190, 2010/11/01/ 2010.

[12] M. Khoshvaght-Aliabadi, S. M. Hassani, and S. H. Mazloumi, "Performance enhancement of straight and wavy miniature heat sinks using pin-fin interruptions and nanofluids," *Chemical Engineering and Processing: Process Intensification,* vol. 122, no. Supplement C, pp. 90-108, 2017/12/01/ 2017.

[13] D. Yang, Z. Jin, Y. Wang, G. Ding, and G. Wang, "Heat removal capacity of laminar coolant flow in a micro channel heat sink with different pin fins," *International Journal of Heat and Mass Transfer,* vol. 113, no. Supplement C, pp. 366-372, 2017/10/01/ 2017.

[14] W. Duangthongsuk and S. Wongwises, "A comparison of the heat transfer performance and pressure drop of nanofluid-cooled heat sinks with different miniature pin fin configurations," *Experimental Thermal and Fluid Science,* vol. 69, no. Supplement C, pp. 111-118, 2015/12/01/ 2015.

[15] S. Ramphueiphad and S. Bureerat, "Synthesis of multiple cross-section pin fin heat sinks using multiobjective evolutionary algorithms," *International Journal of Heat and Mass Transfer,* vol. 118, no. Supplement C, pp. 462-470, 2018/03/01/ 2018.
[16] G. D. Xia, J. Jiang, J. Wang, Y. L. Zhai, and D. D. Ma, "Effects of different geometric structures on fluid flow and heat transfer performance in microchannel heat sinks," *International Journal of Heat and Mass Transfer,* vol. 80, pp. 439-447, 2015/01/01/ 2015.
[17] A. Esmaeilnejad, H. Aminfar, and M. S. Neistanak, "Numerical investigation of forced convection heat transfer through microchannels with non-Newtonian nanofluids," *International Journal of Thermal Sciences,* vol. 75, pp. 76-86, 2014/01/01/ 2014.
[18] N. Raja Kuppusamy, R. Saidur, N. N. N. Ghazali, and H. A. Mohammed, "Numerical study of thermal enhancement in micro channel heat sink with secondary flow," *International Journal of Heat and Mass Transfer,* vol. 78, pp. 216-223, 2014/11/01/ 2014.
[19] B. A. Jasperson, Y. Jeon, K. T. Turner, F. E. Pfefferkorn, and W. Qu, "Comparison of Micro-Pin-Fin and Microchannel Heat Sinks Considering Thermal-Hydraulic Performance and Manufacturability," *IEEE Transactions on Components and Packaging Technologies,* vol. 33, no. 1, pp. 148-160, 2010.
[20] http://www.cree.com/power/products/sic-power-modules/sic-modules/cas100h12am1.
[21] E. R. G. Eckert and R. M. D. Jr, *Analysis of heat and mass transfer*. New-York, USA: McGraw-Hill, 1972.
[22] A. Al-Damook, N. Kapur, J. L. Summers, and H. M. Thompson, "An experimental and computational investigation of thermal air flows through perforated pin heat sinks," *Applied Thermal Engineering,* vol. 89, no. Supplement C, pp. 365-376, 2015/10/05/ 2015.